JACS
JOURNAL OF THE AMERICAN CHEMICAL SOCIETY
pubs.acs.org/JACS
Article

# Spectroscopic Identification of Charge Transfer of Thiolated Molecules on Gold Nanoparticles via Gold Nanoclusters

Mohammad Tavakkoli Yaraki, Noelia Soledad Rubio, Anastasiia Tukova, Junxian Liu, Yuantong Gu, Liangzhi Kou,* and Yuling Wang*

Cite This: J. Am. Chem. Soc. 2024, 146, 5916−5926
Read Online
ACCESS | Metrics & More | Article Recommendations | Supporting Information

**ABSTRACT:** Investigation of charge transfer needs analytical tools that could reveal this phenomenon, and enables understanding of its effect at the molecular level. Here, we show how the combination of using gold nanoclusters (AuNCs) and different spectroscopic techniques could be employed to investigate the charge transfer of thiolated molecules on gold nanoparticles (AuNP@Mol). It was found that the charge transfer effect in the thiolated molecule could be affected by AuNCs, evidenced by the amplification of surface-enhanced Raman scattering (SERS) signal of the molecule and changes in fluorescence lifetime of AuNCs. Density functional theory (DFT) calculations further revealed that AuNCs could amplify the charge transfer process at the molecular level by pumping electrons to the surface of AuNPs. Finite element method (FEM) simulations also showed that the electromagnetic enhancement mechanism along with chemical enhancement determines the SERS improvement in the thiolated molecule. This study provides a mechanistic insight into the investigation of charge transfer at the molecular level between organic and inorganic compounds, which is of great importance in designing new nanocomposite systems. Additionally, this work demonstrates the potential of SERS as a powerful analytical tool that could be used in nanochemistry, material science, energy, and biomedical fields.

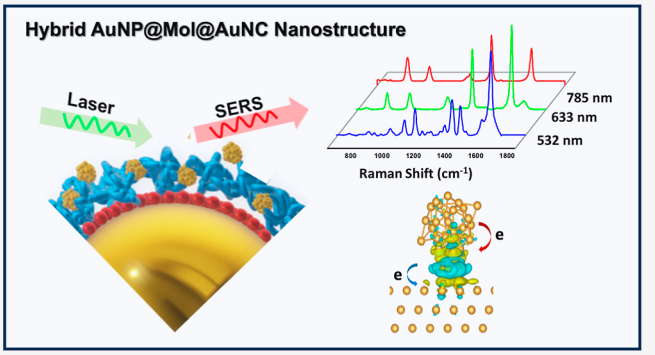


## INTRODUCTION

The advancement in modern science and technology is indebted to the development in analytical chemistry, which provides insight into natural phenomena and enables us to understand the basic regularities behind each.[1,2] Since many advancements are based on designing hybrid nanostructures, analysis of phenomena that occur in hybrid systems has become a crucial step in their development.

Charge transfer plays an important role in designing new nanomaterials and many physicochemical phenomena, leading to recent advancements in energy storage,[3,4] chemical reaction and catalysts,[5] and biosensors.[6,7] Briefly, charge transfer occurs at the interface of hybrid nanostructures, where two nanomaterials form a donor−acceptor pair, and charge in the form of hot electron or hole could be moved from one nanomaterial to another.[8] In recent years, plasmonic nanomaterials (i.e., gold and silver) have received tremendous interest in the synthesis and fabrication of hybrid systems, when they are combined with semiconductors, organic materials, or optical nanomaterials.[9] Plasmonic nanostructures have free electrons that not only contribute to the charge transfer process but also induce charge transfer at the interface of metal-based hybrid systems, owing to their unique feature called localized surface plasmon resonance (LSPR).[9,10] Charge transfer plays an important role in designing new nanomaterials and many physicochemical phenomena, leading to recent advancements in energy storage,[3,4] chemical reaction and catalysts,[5] and biosensors.[6,7]

Understanding the charge transfer process between nanomaterials leads to a rational design with maximum efficiency toward specific applications.[11] Interestingly, Goldmann et al.[12] have investigated the role of charge transfer between thiolated benzoic molecules and gold nanoparticles and its effect on the optical properties of gold nanoparticles. They have employed a combined UV−visible spectroscopy and ellipsometry approach to show how thiolated benzoic molecules could affect the LSPR properties of AuNPs through charge transfer from organic molecule to s-band and d-band electrons in AuNPs. However, this approach did not provide information on what chemical bonds in the molecule could be affected by charge transfer. Charge transfer will not only affect the optical property of gold nanoparticles but also the associated

Received: October 26, 2023
Revised: February 5, 2024
Accepted: February 7, 2024
Published: February 21, 2024

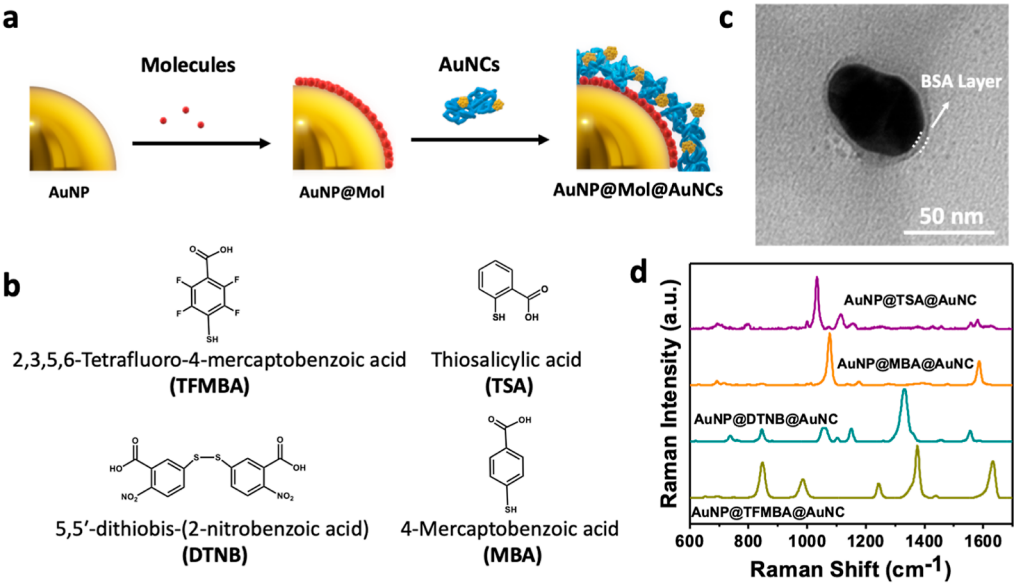


**Figure 1.** (a) Schematic illustration of the preparation of the AuNP@Mol@AuNCs sandwich structure, (b) four different thiolated aromatic molecules and their chemical structures, (c) TEM image of AuNP@TFMBA@AuNCs and corresponding Bovine serum albumin (BSA) layer as a template for AuNCs, and (d) SERS spectra for different AuNP@Mol@AuNC sandwich structures under a 785 nm excitation laser.

molecules (i.e., thiolated benzoic molecule). Therefore, new analytical approaches are still needed to shed light on this aspect of charge transfer in the hybrid system and provide deeper insight into the charge transfer process at the interface of hybrid systems.

Raman spectroscopy is a noninvasive technique that provides information about the vibration of different bonds in the molecules. Since the Raman scattering is inherently weak, the amplification of Raman scattering is of great importance.[7,13] Surface-enhanced Raman scattering (SERS) could enable this by amplification of Raman signals by several orders of magnitude, when the molecule is adsorbed on the surface of plasmonic (i.e., noble metals such as gold and silver[14−16]) or nonplasmonic (i.e., metal oxide semiconductors and 2D nanomaterials[17,18]) nanomaterials. There are two main mechanisms that explain the SERS effect. The electromagnetic (EM) enhancement (i.e., plasmon-enhanced mechanism) is the main mechanism when the molecule is adsorbed on the surface of plasmonic nanomaterials. Noble metals with a size of less than 100 nm have free electrons that start oscillating when they are being hit by light (i.e., EM wave) with a wavelength larger than the size of noble metal nanoparticles. The oscillation of free electrons results in an enhanced electric field around metal nanoparticles. Since the optical properties of molecules (i.e., excitation, scattering, etc.) depend on the magnitude of the electric field in the environment, the Raman signal of the adsorbed molecule on the surface of metal nanoparticles could be amplified proportionally to the fourth power of the enhanced electric field.[19] Another mechanism is chemical enhancement (i.e., mostly through charge transfer), which is the main mechanism in nonplasmonic SERS systems.[20] Although the contribution of the chemical enhancement mechanism is less than EM enhancement in plasmonic SERS systems, it sometimes is not negligible.[21] Since the chemical enhancement via charge transfer between nanomaterial (adsorbent) and adsorbed molecules is one of the mechanisms that has been identified to explain the SERS effect, SERS could be employed not only to investigate the charge transfer process between molecules and nanomaterials but also to understand the phenomenon of charge transfer in hybrid systems. Additionally, the SERS-based system is also employed as an analytical tool for biomedical applications as well as in other fields such as environment, energy, and optoelectronics.

Metal nanoclusters (i.e., Au, Ag, and Cu) with their unique optical properties and molecule-like behavior have demonstrated high efficacy in the charge transfer process.[22−24] However, metal nanoclusters' chemical enhancement mechanism (via charge transfer) potential in SERS systems has not been investigated. Due to the importance of increased SERS signals in designing SERS nanostructures for high sensitivity,[25−27] taking advantage of both (EM, using plasmonic nanoparticles) charge transfer mechanisms seems to be a promising approach that has not received much attention yet.

In this work, for the first time, we report how introducing Au nanoclusters (AuNCs) could modulate the Raman spectrum of a molecule (Mol) adsorbed on the surface of gold nanoparticles (AuNPs) in an AuNP@Mol@AuNCs sandwich structure. To do this, we used four different thiolated-aromatic compounds with a similar binding chemistry (i.e., thiol group) to the surface of AuNP. The charge transfer process was confirmed by excitation wavelength-dependent Raman spectroscopy in all four samples. Furthermore, a series of density functional theory (DFT) calculations were performed to show how the presence of AuNCs affects the Raman spectra and their intensity in different molecules through the charge transfer process. We believe that the proposed design of AuNC-enabled charge transfer for SERS and fundamental studies on the interaction between AuNCs and different molecules could open a new avenue to the future application of SERS in colloidal systems as well as other fields such as energy and material science.

## RESULTS AND DISCUSSIONS

**Synthesis and Characterization of AuNP@Mol@AuNCs.** The new AuNP@Mol@AuNC sandwich structures were established via a two-step procedure, as shown in Figure


https://doi.org/10.1021/jacs.3c11959
J. Am. Chem. Soc. 2024, 146, 5916−5926

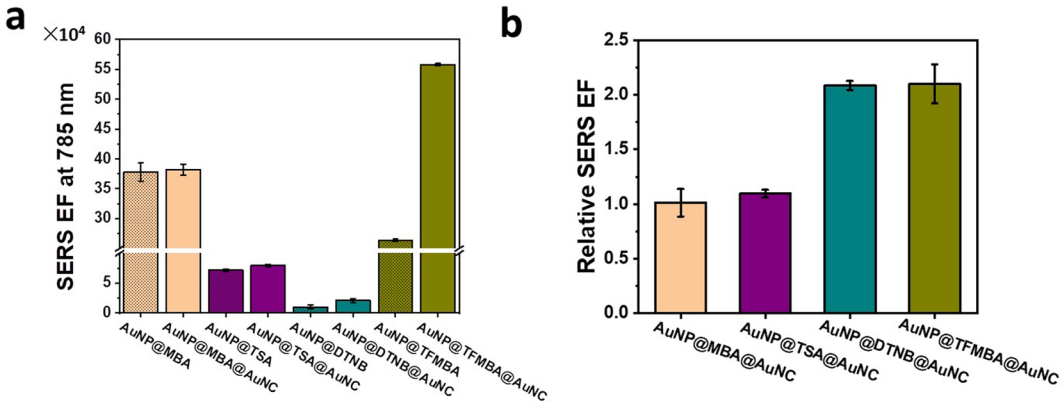


**Figure 2.** (a) Calculated SERS EFs for different samples at 785 nm and (b) relative SERS EF for different AuNP@Mol@AuNC samples at 785 nm. The average and standard deviation are for replicate measurements ($n$ = 3).

1a. Citrate-capped AuNPs with a relatively homogeneous spherical shape and average size of (56 ± 9 nm by transmission electron microscopy (TEM)) (Figure S1a) were synthesized by the Turkevich method.[28] The obtained suspension of AuNPs had a purple color with a hydrodynamic diameter of 56.26 ± 0.05 nm obtained by nanoparticle tracking analysis (NTA) (Figure S1b). The maximum localized plasmon resonance peak at 532.6 nm (Figure S1c) is in agreement with previous studies.[28−30]

To prepare AuNP@Mol@AuNCs sandwich structures, four different thiolated aromatic molecules [i.e., 5,5′-dithiobis(2-nitrobenzoic acid) (DTNB), 4-mercaptobenzoic acid (MBA), 2,3,5,6-Tetrafluoro-4-mercaptobenzonic acid (TFMBA), and thiosalicylic acid (TSA)] containing thiol group and carboxylic group were used (Figure 1b). These molecules could bind to the AuNP surface through the Au−S covalent bond[31] to form molecule-conjugated AuNP (AuNP@Mol, see Table S1 for a conjugation condition). The amount of each molecule was selected carefully to obtain stable AuNP@Mol samples (Figure S2). The conjugation of molecules on AuNPs caused a few nanometers red-shift in the LSPR peak of AuNPs, as well as an increase in hydrodynamic size (Figure S1b). The average hydrodynamic size of AuNPs increased from 56.26 to 57.56 nm (AuNP@DTNB), 60.90 nm (AuNP@TFMBA), 63.1 nm (AuNP@MBA), and 59.03 nm (AuNP@TSA), which confirms the successful conjugation of thiolated aromatic molecules on the AuNP surface and changes in the refractive index of the environment at the surface of AuNPs. The as-prepared AuNP@Mol nanoparticles demonstrated SERS enhancement and had a specific SERS spectrum for each of the AuNP@Mol samples, as shown in Figure S1d. The obtained peaks for each AuNP@Mol sample are well-matched with the corresponding peaks in molecules (Table S2). To quantitatively assess the SERS enhancement, the SERS enhancement factor (EF) was calculated using TFMBA as an example (see the details in Supporting Information-1), which shows the SERS EF of 2.64 × $10^5$ of TFMBA on AuNPs in solution.

BSA was used as a template for the synthesis of AuNCs, which occurs at alkaline conditions (pH = 11−12). In this reaction, BSA acts as both a mild reducing agent and a template for AuNC growth. BSA has a globular structure with a cavity inside. In particular, site-I located in the hydrophobic cavity of subdomain IIA has been shown as a specific site for interaction and complexation with metal ions.[32,33] It is believed that this cavity is responsible for the formation of nanoclusters within the BSA protein, which is evidenced by the high stability of protein-templated metal nanoclusters. BSA has 21 Tyrosine residues that reduce $Au^{3+}$ ions slowly to $Au^0$ atoms and the BSA template covers the surface, preventing the further growth of AuNCs; the number of $Au^0$ atoms in BSA-templated AuNCs is approximately 25 atoms per cluster.[34] In theory, two BSA molecules contain one Au cluster. However, there are fewer clusters because BSA has been used as the reducing reagent and capping (template) reagent. Therefore, each BSA molecule may not have more than one cluster. The obtained AuNC suspension had a bright orange−brown color (Figure S3a). The as-synthesized BSA−AuNCs had a red-color fluorescence emission ($\lambda_{emission}$ = 620 nm, Figure S3a), which is due to the quantum confinement effect in AuNCs.[34] As can be seen in Figure S3b, the as-synthesized BSA−AuNCs possess a small size around 2 nm, which is in agreement with the size of Au atom (i.e., 0.146 nm) and the number of Au atoms (i.e., 25) reported by Xie et al.[34] This confirms the successful formation of Au nanoclusters containing 25 atoms inside the BSA as the template. BSA−AuNCs showed a strong fluorescence background (Figure S3c) and a very weak Raman signal (Figure S3d) under different excitation wavelengths, within which the weak signals were from BSA molecules (Table S3).

Incubation of AuNP@Mol with BSA−AuNCs (see Table S4) resulted in the formation of a thin layer of BSA−AuNCs (∼7 nm equal to the size of BSA molecule[35]) on the surface of AuNP@Mol, which can be seen in the TEM image presented in Figure 1c. This happens due to the binding of BSA on the AuNPs via electrostatic interaction as well as the interaction between disulfide and cysteine groups in BSA and the surface of AuNP (i.e., AuNP@Mol has a pH of 6−7 and AuNCs are in alkaline pH).[36] The conjugation of BSA-AuNCs to AuNP@Mol nanoparticles was further confirmed by NTA and UV−vis spectroscopy. An increase in the hydrodynamic sizes of all AuNPs after incubation with BSA−AuNCs as well as a red-shift in the LSPR peak of AuNPs indicate the successful adsorption of BSA−AuNCs on the surface of different AuNP@Mol samples (Figure S4). The red-shift in the LSPR peak is due to an increase in the refractive index of the surrounding environment (BSA, $n$ = 1.602) compared to bare AuNPs (water, $n$ = 1.33), which was further confirmed by simulation results for extinction spectra of AuNP and AuNP@BSA (Figure S5). Additionally, all AuNP@Mol@AuNC structures had a smaller zeta potential value compared with their


https://doi.org/10.1021/jacs.3c11959
J. Am. Chem. Soc. 2024, 146, 5916−5926

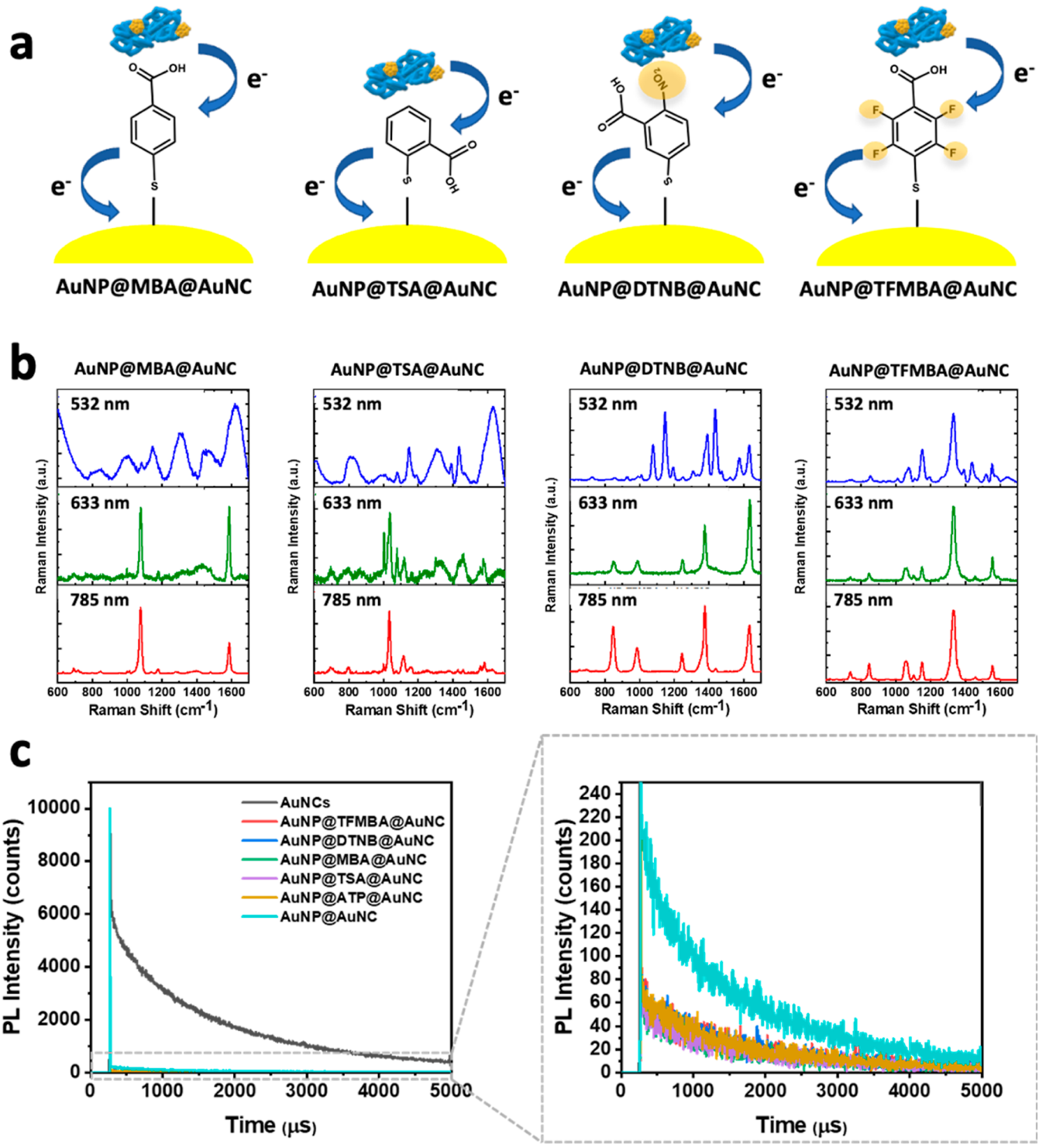


**Figure 3.** (a) Scheme of the charge transfer process in AuNP@Mol@AuNC SERS nanostructures. The highlighted functional groups in DTNB and TFMBA are electron-withdrawing groups. (b) Excitation-dependent SERS spectra in different AuNP@Mol@AuNC sandwich structures. The strong fluorescence background under 532 nm suppressed the Raman signature of TSA and MBA. (c) Fluorescence lifetime for AuNCs before and after adsorption on the surface of AuNP@Mol and AuNP samples.

corresponding AuNP@Mol samples, showing that BSA-templated AuNCs have been successfully adsorbed on the surface of AuNP@Mol samples (Table S5). The as-synthesized AuNP@Mol@AuNC structures possessed the same Raman signature as AuNP@Mol samples (Figure S1d, after baseline correction), indicating that the presence of AuNCs has a negligible effect on the Raman spectra profiles of the molecules in terms of peak positions (Figure 1d).

**Effect of AuNCs on the SERS Intensity of AuNP@Mol.** A fixed thickness (~7 nm) of BSA−AuNCs was employed in this study because of the nature of chemical reaction and interaction between BSA-templated AuNCs and AuNPs@Mol, which makes it challenging to tune the thickness. The initial



https://doi.org/10.1021/jacs.3c11959
J. Am. Chem. Soc. 2024, 146, 5916−5926

amount of AuNCs might affect the amount of adsorbed AuNCs on the surface of AuNP@Mol, in turn leading to different degrees of amplification of SERS intensity. It was observed that the SERS intensities in AuNP@DTNB@AuNCs and AuNP@TFMBA@AuNCs gradually improved with the increase in the amount of BSA−AuNCs and reached a plateau, designating the formation of a layer of BSA−AuNCs on the surface of AuNP@Mol. However, such a trend was not found in the case of MBA- and TSA-functionalized nanoparticles (Figure S6). These results suggest that when there are enough AuNCs to be adsorbed on AuNP@Mol, SERS intensity will be maximized, which is due to the charge transfer effect enabled by AuNCs. As can be seen in Figure 2a, the coating of AuNCs on AuNP@Mol results in greater SERS EFs of $5.3 \times 10^4$ (AuNP@TSA@AuNC), $2.5 \times 10^5$ (AuNP@MBA@AuNC), $3.8 \times 10^4$ (AuNP@TFMBA@AuNC), and $1.4 \times 10^5$ (AuNP@DTNB@AuNC) under a 785 nm Raman laser. In particular, SERS amplification for the samples containing TFMBA and DTNB was about 2-fold at optimized conditions, while it was around 10% in TSA and less than 3% in MBA (Figure 2b).

The differences in the observed SERS amplification in samples containing different molecules can be explained by the structural features of these molecules and the different extent of charge transfer from the molecules to the surface of AuNPs. As illustrated in Figure 3a, charge transfer from AuNCs to the molecules can occur, which results in the improvement of the SERS signal (Figure 2b). In the case of MBA and TSA, this charge transfer is weakly altered, leading to less than 10% amplification in their SERS signal in AuNP@Mol@AuNC structure. In contrast, TFMBA and DTNB have electron-withdrawing groups that change the polarizability of the molecules.[37] The polarizability of the molecule has a direct effect on the Raman scattering, and it is a function of the electric field of the environment. Therefore, we hypothesize that the plasmonic effect from AuNPs could alter the polarizability and improve the SERS signal.[38,39] In addition, it has been found that polarized molecules could accelerate the charge transfer process in their binary complex with other molecules.[40,41] These molecular structure differences might be a possible reason leading to larger improvement of SERS signals in AuNP@TFMBA@AuNC and AuNP@DTNB@AuNC samples.

To confirm that chemical mechanism (i.e., via charge transfer) is involved in the observed SERS improvement, and presence of AuNCs leads to occurring charge transfer in all AuNP@Mol@AuNC sandwich structures, excitation wavelength-dependent SERS was investigated. The excitation laser and its overlap with the bandgap (the energy difference between the highest occupied molecular orbital and the lowest unoccupied molecular orbital) of each molecule could affect the Raman signature of the molecule through charge transfer process. This appears as changes in the intensity of the main peaks as the result of different resonances under different excitation wavelengths. Also, the stronger resonance of some bond vibrations (i.e., ring) under excitation wavelengths with higher energy (i.e., 633 and 532 nm compared to 785 nm) leads the corresponding vibrations to become more visible in the Raman spectra.[42] Similar results have been found by Shan et al.,[43] where methylene blue chemisorbed on $Nb_2O_5$ nanoparticles showed different levels of resonance and, therefore, different Raman signatures as a function of excitation laser wavelength. As can be seen in Figure 3b, the ratio between the characteristic peaks of the thiolated aromatic molecules was changed when the excitation wavelength changed[25] (raw spectra are presented in Figure S7). To perform a more in-depth analysis of Raman spectra of different molecules, DFT calculations were used to assign the peaks (Figure S8), and the results of the analysis are presented in Table S6.

In particular, MBA possesses two main peaks at 1077 $cm^{-1}$ (aromatic ring vibration and C−S stretching) and 1587 $cm^{-1}$ (aromatic C═C stretching). While the aromatic C═C stretching peak is weaker under 785 nm excitation, it has a similar intensity to the other peak under 633 nm excitation. Similarly, the aromatic C═C stretching vibration at 1583 $cm^{-1}$ in TSA also becomes stronger when the excitation laser is changed from 785 to 633 nm. Although we did not observe significant improvement in SERS signals in both AuNP@MBA@AuNC and AuNP@TSA@AuNC, the charge transfer process occurs in these two samples, evidenced by changes in the ratio of the main peaks in both MBA and TSA as a function of laser excitation wavelength.[42,44,45] In addition, the fluorescence background under the 532 nm excitation laser is strong, and therefore, it suppresses the weak Raman signals for the vibration of different bonds in TSA and MBA molecules.

Interestingly, charge transfer amplified some of the vibrations when samples containing TFMBA and DTNB were excited by the 532 nm laser, making them more visible in the SERS spectra. In DTNB, while the symmetric nitro-group stretching peak at 1337 $cm^{-1}$ is dominant under all excitation wavelengths, the intensity of other vibrations changes by changing the excitation wavelength, where in particular, aromatic C−H in-plane vibration at 1150 $cm^{-1}$ and C−H scissoring (in $CH_2$) at 1456 $cm^{-1}$ become relatively stronger by decreasing the excitation wavelength. In TFMBA, OH. O out-of-plane deformation becomes weaker compared to other peaks when the excitation laser changes from 785 to 633 and 532 nm. Additionally, the C═O stretching peak at 1633 $cm^{-1}$ becomes weaker than the peak at 1376 $cm^{-1}$ (ring stretching/C−F stretching), when the excitation wavelength is changed from 785 to 633 nm. The peaks at 1077 $cm^{-1}$ (C−S), 1147 $cm^{-1}$ (CCC ring deformation), 1193 $cm^{-1}$ (CCC Ring deformation), and 1573 $cm^{-1}$ (CCC ring deformation) could be only found in the spectrum of AuNP@TFMBA@AuNCs when we excite them by 532 nm. Although all bonds vibrate under all three excitation wavelengths, some are stronger than others and suppress the weaker signals.[46] However, by introducing AuNCs and a stronger charge transfer effect, vibrations related to ring deformation and C−S become more visible since the molecule resonates in different ways. A similar observation has been reported in 4-methoxythiophenol adsorbed on the surface of gold nanoring when the excitation wavelength changed from 785 to 633 and 532 nm.[42] In another work, Richter et al.[45] have reported the appearance of Raman peaks for *p*-aminothiophenol (4-ATP) in a Ag colloids@4-ATP/ZnO junction, when excitation wavelength decreased from 1064 to 514.5 nm. The excitation wavelength with a higher energy has a higher chance of resonating with the donor (i.e., ZnO in Richter et al.'s work and AuNCs in this work), enabling a better charge transfer process. In particular, the 532 nm laser is closer to the absorption wavelength of AuNCs used in this study (470 nm, see Figure S3a), enabling a higher degree of excitation in AuNCs, and in turn, providing more electrons to be transferred to surrounding molecules in the AuNP@Mol@AuNC system. These excitation wavelength-


https://doi.org/10.1021/jacs.3c11959
J. Am. Chem. Soc. 2024, 146, 5916−5926

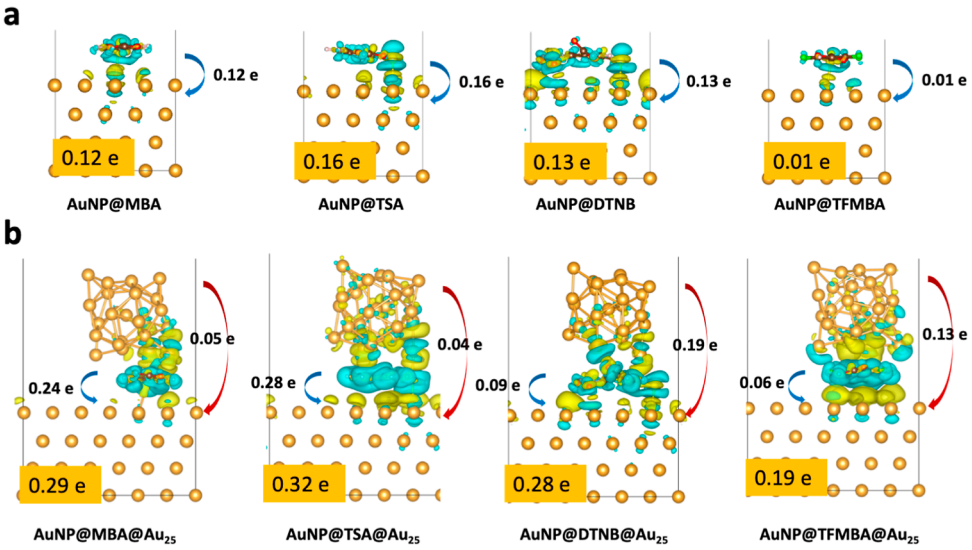


**Figure 4.** Schematic representation of the charge transfer process obtained via DFT calculations for (a) AuNP@Mol structures and (b) AuNP@Mol@AuNC sandwich structures. The blue arrow indicates the net charge transfer from the thiolated aromatic molecule. The red arrow indicates the net charge transfer from AuNC. The orange box indicates the net charge that AuNP is receiving.

dependent SERS spectral features show that charge transfer plays a crucial role in the AuNP@Mol@AuNC system.

Additionally, we compared the SERS spectra obtained for AuNP@Mol@AuNC samples with the corresponding AuNP@Mol samples (see Figure S9 for SERS spectra of AuNP@Mol samples). As can be seen in Figure S10, samples containing MBA and TSA were less sensitive to the presence of AuNCs compared to the samples containing TFMBA and DTNB. In samples containing TFMBA and DTNB, an obvious red-shift was observed in the SERS peak position corresponding to the C−F stretching (1367 $cm^{-1}$) and symmetric nitro-group stretching (1337 $cm^{-1}$), respectively. The shift in Raman frequency is usually attributed to the change in the chemical environment.[47] However, we observed a significant shift in AuNP@TFMBA@AuNC and AuNP@DTNB@AuNC, the two samples, which we observed SERS improvement. Ma et al.[48] have also observed that charge transfer could affect the Raman frequency. Since all AuNP@Mol@AuNC samples contain a layer of BSA-templated AuNCs, the chemical environment for Raman molecules could be considered similar. Therefore, the significant shift in the position of the Raman peak in TFMBA and DTNB could be possibly due to a stronger charge transfer effect in the samples containing these two molecules.[49] We further investigated the changes in the ratio between the two dominant SERS peaks in each AuNP@Mol and AuNP@Mol@AuNC samples under different Raman excitation wavelengths (Figure S11). Charge transfer usually affects the vibration in different bonds and leads to a change in their frequency. In particular, charge transfer affects the benzene ring and chemical bonds attached to the benzene ring (C−S bond or functional groups on benzene rings) differently. Therefore, it is expected that in a system with charge transfer, the ratio between the SERS peaks changes[50] and becomes wavelength-dependent.[51] The results show that the ratios between the SERS peaks were affected by the presence of AuNCs in the system, indicating that charge transfer could occur in all samples and AuNCs have contributed to changing the SERS spectra through the charge transfer process. Park et al.[52] have shown that the formation of a molecular junction could lead to charge transfer, and in turn, a different resonance in the trapped molecule between two nanomaterials. In our study, the molecule is also trapped between AuNP and AuNCs, forming a molecular junction, which might be the reason behind the changes in the ratios between the SERS peaks.

The charge transfer between AuNCs and AuNP@Mol was further confirmed by analysis of the fluorescence lifetime of AuNCs before and after adsorption on AuNP@Mol (Figure 3c). While AuNCs are highly emissive in their free solution, it was observed that AuNP@AuNC and AuNP@Mol@AuNC samples were almost nonemissive. The strong quench in fluorescence intensity in all samples indicates the energy transfer from excited AuNCs to AuNP@Mol. The main mechanism for this process is nanometal surface energy transfer (NSET) when an excited fluorophore in the vicinity of a metal nanoparticle could pass its energy to the surface of metal nanoparticle with insufficient spectral overlap between its fluorescence spectrum and extinction spectrum of metal nanoparticle.[53] Such a charge transfer results in quenched fluorescence in the fluorophore,[54] which is in agreement with our observation in this study. Similarly, the average fluorescence lifetime of AuNCs (1.83 $\mu$s) decreased to 1.278 $\mu$s (AuNP@TFMBA@AuNCs), 1.312 $\mu$s (AuNP@DTNB@AuNCs), 1.273 $\mu$s (AuNP@MBA@AuNCs), and 1.318 $\mu$s (AuNP@TSA@AuNCs), indicating the charge transfer from AuNCs to AuNP@Mol. The fluorescence lifetime (i.e., defined as $\frac{1}{(k_r + k_{nr})}$) is inversely proportional to the summation of radiative decay rate ($k_r$) and nonradiative decay rate ($k_{nr}$). Although both of these decay rates increase dramatically when the fluorophore (i.e., AuNCs) is in close distance from the surface of the metal nanoparticle, the increase in $k_{nr}$ is much more than the increase in $k_r$, leading to fluorescence quenching and a decrease in fluorescence lifetime.[55,56] Interestingly, the decrease in the average fluorescence lifetime of AuNCs in AuNP@Mol@AuNC samples was more than AuNP@AuNC (1.352 $\mu$s), denoting the role of Mol in the acceleration of charge transfer between AuNCs and AuNPs.

In order to better understand the charge transfer process in AuNP@Mol@AuNC sandwich structures and how the


https://doi.org/10.1021/jacs.3c11959
J. Am. Chem. Soc. 2024, 146, 5916−5926

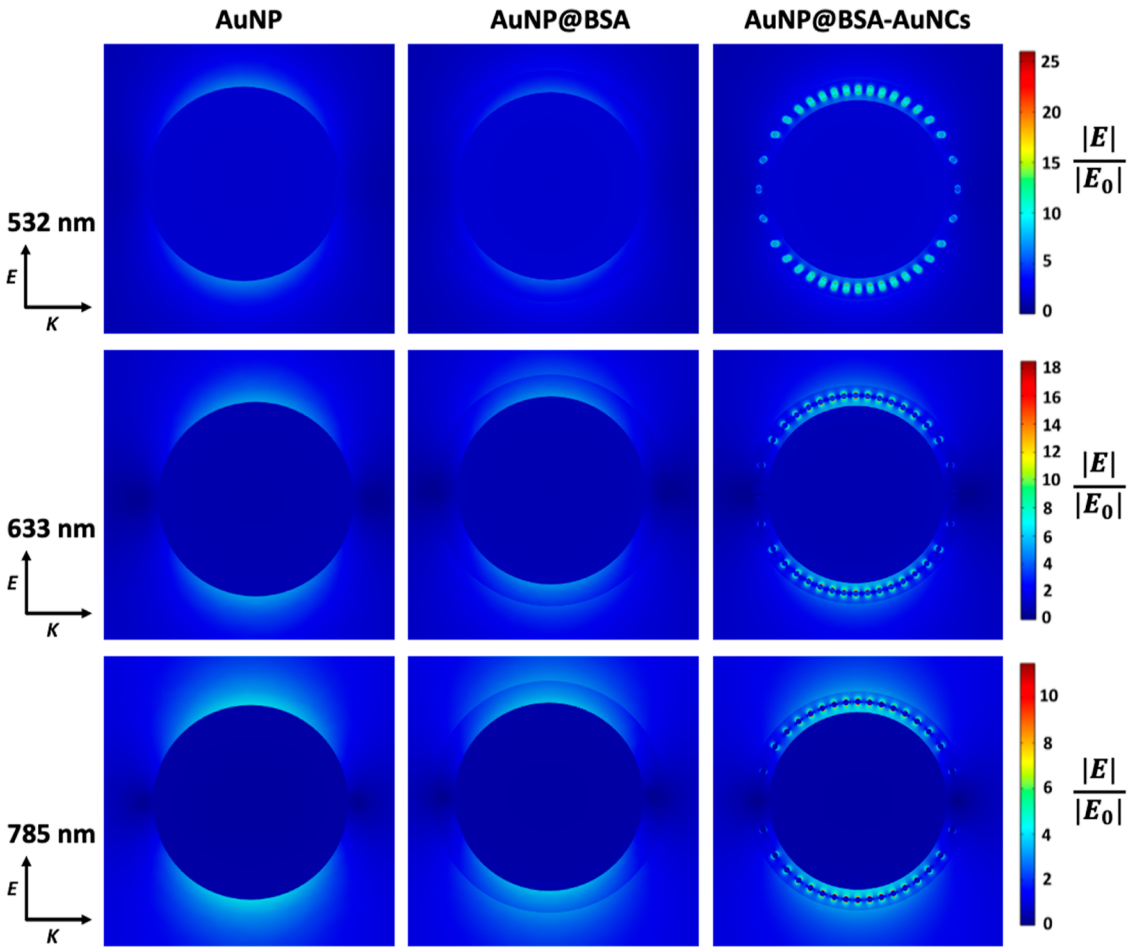


**Figure 5.** Simulated enhanced electric field ($\frac{|E|}{|E_0|}$) distribution around AuNP, AuNP@BSA, and AuNP@BSA−AuNCs under incident light with different wavelengths (532, 633, and 785 nm). *E* indicates the polarization direction and *K* indicates the direction of light propagation. The diameter of AuNP was designed as 50 nm and the diameter of AuNCs was designed as 2 nm.

presence of AuNC modulates the Raman signal from the adsorbed molecules on the surface of AuNPs, the corresponding DFT computations were performed (see Figures S12−S14 for optimized structures). The results for AuNP@Mol systems show that all adsorbed molecules lose electrons, which is accepted by AuNPs (Figure 4a). The difference between the calculated net charge transfer rates is due to the nature of molecules and their different optoelectronic properties.[57] In AuNP@Mol@AuNC sandwich structures, both molecules and AuNC lose electrons, and these lost electrons are received by AuNP (Figure 4b). The net charge transfer in the molecules is clearly affected by the presence of the Au nanocluster, confirming that charge transfer mechanism is involved in the SERS recorded for different samples under different excitation wavelengths (Figure 3b).

In particular, MBA and TSA lose more electrons (i.e., 0.24 and 0.28 $e^-$ for MBA and TSA, respectively) than DTNB and TFMBA (i.e., 0.09 and 0.06 $e^-$ for DTNB and TFMBA, respectively). These results could be correlated to the SERS spectra recorded at 532 nm excitation wavelength (Figure 3b, blue spectra), where the weak Raman signal of TSA and MBA was suppressed by the strong fluorescence background from AuNCs. The spectra shown in Figure 3b under 532 nm come from BSA molecules in the BSA-templated AuNCs. Indeed, the fluorescence background from BSA−AuNCs suppresses the SERS intensity of MBA and TSA, and therefore, only SERS of BSA is observable after baseline correction. In contrast, DTNB and TFMBA possessed distinct Raman signals when they were irradiated with a 532 nm laser. It is worth mentioning that the SERS enhancement at 532 nm for the samples with AuNP core is mainly due to the charge transfer process since AuNPs need incident light with longer wavelength to show EM mechanism-based SERS.[25] Such an observation indicates that modulation of the net charge transfer rate in the molecules in the presence of AuNCs is a key factor in observing SERS via chemical (charge transfer) enhancement mechanism.

Interestingly, the DFT results also show that AuNC loses more electron/charge in AuNP@DTNB@AuNC and AuNP@TFMBA@AuNC sandwich structures compared with AuNP@MBA@AuNC and AuNP@TSA@AuNC structures (red arrows in Figure 4b). This charge transfer might be through the adsorbed molecules or directly to the surface of AuNP. The electron/charge transferred from AuNC is eventually received by AuNP, leading to an increase in surface charge density on the surface of AuNP. The higher surface charge density in AuNP@DTNB@AuNC and AuNP@TFMBA@AuNC sandwich structures results in stronger enhancement of the EM field around AuNP, leading to further SERS amplification due to EM enhancement mechanism.


https://doi.org/10.1021/jacs.3c11959
J. Am. Chem. Soc. 2024, 146, 5916−5926

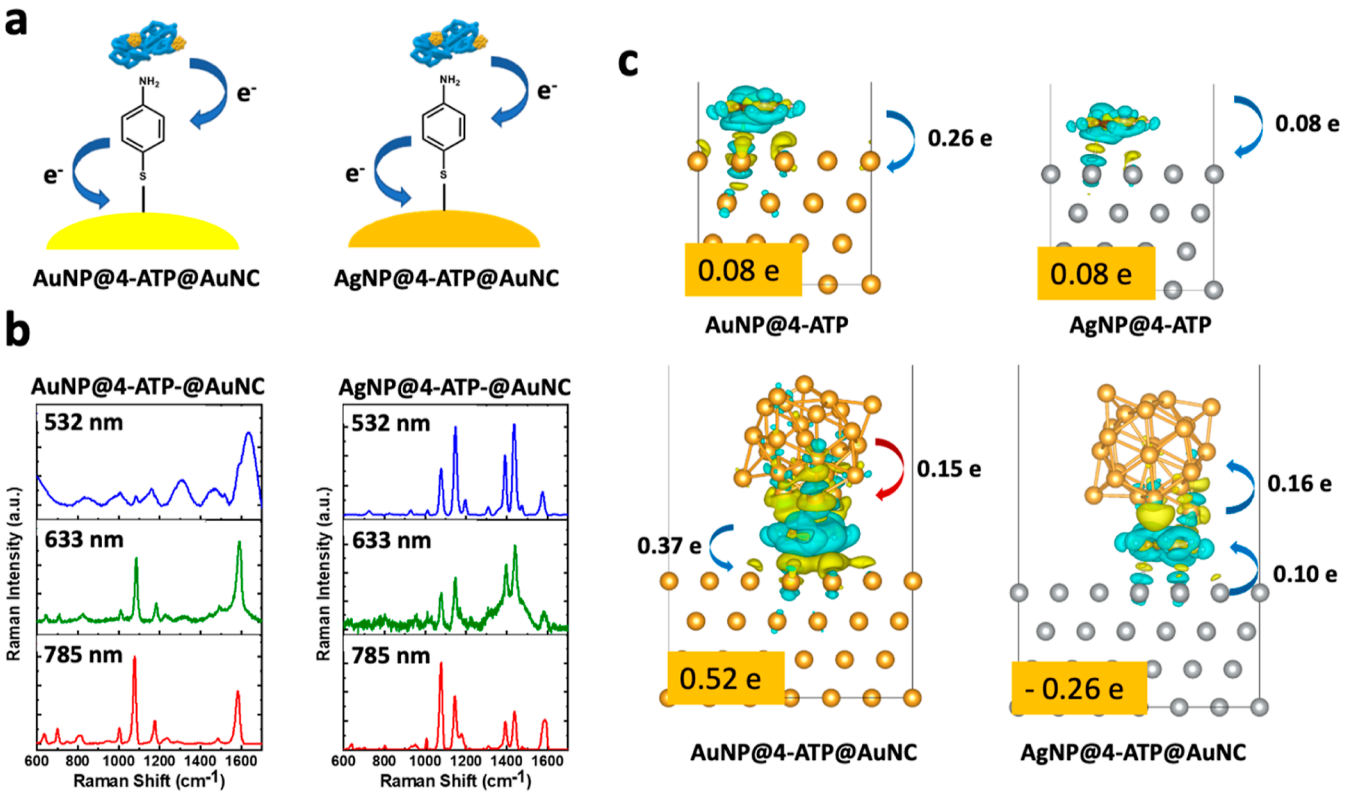


**Figure 6.** Possible charge transfer process (a) and excitation-dependent SERS spectra (b) in AuNP@ATP@AuNC and AgNP@ATP@AuNC structures and (c) DFT calculation for charge transfer from the $Au_{25}$ nanocluster to ATP and from ATP to the Au(111) surface.

To further investigate the possible mechanisms involved in the observed SERS amplification, the electric field around AuNPs was simulated in the presence and absence of the layer of BSA-AuNCs around AuNPs under different excitation wavelengths. As can be seen in Figure 5, the presence of BSA did not significantly change the enhanced electric field around AuNP; however, the presence of AuNCs around AuNPs led to about 14-fold maximum electric field enhancement for 785 nm incident light. Around AuNP compared to bare AuNP (about 4-fold maximum electric field enhancement) for 785 nm incident light. It should be noted that the hotspot in the AuNP@BSA-AuNC system is located closer to the surface of clusters, leading to less electric field enhancement (around 6-fold) on the surface of AuNP, where the molecules are adsorbed. This value still is greater than bare AuNP (about 4-fold maximum electric field enhancement) for 785 nm incident light, indicating the contribution of the EM enhancement mechanism in SERS amplification. The same trend was observed for 633 and 532 nm incident light. These results indicate that the EM mechanism also plays a crucial role in SERS improvement in the AuNP@Mol@AuNC system, and the observed SERS improvements are due to the combination of both EM and charge transfer mechanisms. It has also been reported that the enhanced electric field of the environment could improve the charge transfer process in donor−acceptor systems.[58,59] Such a phenomenon could further alter the charge transfer enhancement observed in the AuNP@Mol@AuNC sandwich structures.

To further verify our hypothesis and the observed results for improved SERS in AuNP@Mol@AuNC sandwich structures, we selected another aromatic thiol molecule, 4-aminothiolphenol (4-ATP), since it has shown promising charge transfer characteristics in the previous SERS studies.[60,61] The excitation wavelength-dependent SERS study (i.e., 532, 633, and 785 nm) on AuNP@4-ATP@AuNC confirms the charge transfer process in this molecule since the ratio between the dominant Raman peaks in Raman spectra of 4-ATP has been clearly changed (Figures 6a,b and S15). The observed trend is in agreement with previous works for analysis of SERS spectra of 4-ATP molecules adsorbed on the metal surface.[62,63] Different excitation wavelength provides different amounts of energy to be absorbed by either AuNP or AuNCs, leading to different degrees of charge transfer in the AuNP@ATP@AuNC system. Additionally, different excitation wavelengths may resonate with different molecular transitions.[64] The DFT results also revealed the charge transfer in the AuNP@4-ATP and AuNP@4-ATP@AuNC systems, where introducing AuNCs to AuNP@4-ATP results in changes of the charge transfer process in this structure. In particular, the charge transfer from 4-ATP to AuNP increased from 0.26 to 0.37 e, where AuNCs also further transferred 0.15 e to this system. This leads to an overall charge of 0.52e received by AuNP in the AuNP@4-ATP@AuNC system. In another experiment, AuNP in the sandwich structure was replaced by Ag nanoparticles (AgNPs) to further investigate the role of AuNCs in enabling the charge transfer independent of the type of the metal core. The replacement of the core led to the SERS spectrum with different patterns under 532 nm, which arises from both chemical enhancement (via charge transfer) and EM enhancement mechanisms (Figure S16 for simulation of enhanced electric field). AgNPs have different absorption and scattering cross sections compared with AuNPs; therefore, a strong enhanced electric field may be observed at 532 nm excitation and, in turn, a plasmon enhancement effect (Figure


https://doi.org/10.1021/jacs.3c11959
J. Am. Chem. Soc. 2024, 146, 5916−5926

S15). Additionally, different excitation wavelengths may resonate differently with the molecule−metal charge−transfer transition, leading to different SERS patterns under different excitation wavelengths as well as using different metal cores.[65]

Furthermore, the ratio between the dominant peaks in Raman spectra of 4-ATP was affected by changing the metal core (i.e., from gold to silver), indicating charge transfer process occurs differently in the AgNP@4-ATP@AuNC sandwich structure. While the AuNC was an electron donor in the AuNP@4-ATP@AuNC system, it acts as an electron acceptor in the AgNP@4-ATP@AuNC system (Figures 6c and S17). This different direction for the charge transfer process could affect the molecular transitions and vibrations in 4-ATP molecules, leading to different SERS spectra for 4-ATP in AgNP@4-ATP@AuNC and AuNP@4-ATP@AuNC systems.

## CONCLUSIONS

In this work, we have proposed a new concept using AuNCs to enable the charge transfer via molecules on AuNPs. By taking advantage of the synergic effect between EM enhancement mechanism and charge transfer enhancement mechanism, it has been shown that AuNCs have the potential to further improve the Raman signal of thiolated aromatic molecules on AuNPs. In particular, it was found that AuNCs can improve the Raman signals of TFMBA and DTNB in the Au@Mol@AuNCs design, while they had less effect on SERS signals of TSA and MBA molecules in similar designs. The larger SERS improvement in AuNP@TFMBA@AuNCs and AuNP@DTNB@AuNCs can be attributed to the presence of electron-withdrawing groups ($NO_2$ and F) in DTNB and TFMBA, respectively. These electron-withdrawing groups could change the polarizability of the thiolated benzene ring (i.e., which is similar in all studied molecules), resulting in a higher level of SERS improvement in both DTNB and TFMBA compared to MBA and TSA molecules. The DFT calculations also showed that AuNCs pump electrons into the surface of the metal nanoparticles, leading to an increase in surface charge density, which could result in higher enhancement of the EM field. The wavelength-dependent SERS study further confirmed the charge transfer mechanism, since the ratio between the Raman peaks in different thiolated aromatic molecules changed under lasers with different excitation wavelengths. In particular, excitation of AuNP@TFMBA-AuNC and AuNP@DTNB-AuNC by 532 nm laser leads to stronger vibration in ring and C−S bonds and making them more visible (i.e., compared to 633 and 785 nm excitation lasers which are being suppressed by other strong vibrations), which confirms the contribution of charge transfer from AuNCs and involvement of charge transfer mechanism in the observed SERS spectra. Our findings clearly demonstrate that AuNCs could enable charge transfer in the hybrid system and affect the SERS signature of the molecules. Additionally, SERS could be employed as a powerful analytical tool to investigate the charge transfer process between molecules in inorganic−organic nanocomposites, which have found their places in many applications in nanochemistry, material science, energy, catalysis, and biomedical fields.

## ASSOCIATED CONTENT

### Supporting Information

The Supporting Information is available free of charge at https://pubs.acs.org/doi/10.1021/jacs.3c11959.

Experimental details, materials, and methods, calculation of SERS EF, Raman spectra before background correction, additional FEM simulation results, and optimized structures for DFT calculations (PDF)

## AUTHOR INFORMATION


### Corresponding Authors

**Liangzhi Kou** − *School of Mechanical, Medical and Process Engineering, Queensland University of Technology, Brisbane, Queensland 4001, Australia;* orcid.org/0000-0002-3978-117X; Email: liangzhi.kou@qut.edu.au

**Yuling Wang** − *School of Natural Sciences, Faculty of Science and Engineering, Macquarie University, Sydney, NSW 2109, Australia;* orcid.org/0000-0003-3627-7397; Email: yuling.wang@mq.edu.au

### Authors

**Mohammad Tavakkoli Yaraki** − *School of Natural Sciences, Faculty of Science and Engineering, Macquarie University, Sydney, NSW 2109, Australia;* orcid.org/0000-0002-6987-7885

**Noelia Soledad Rubio** − *School of Natural Sciences, Faculty of Science and Engineering, Macquarie University, Sydney, NSW 2109, Australia*

**Anastasiia Tukova** − *School of Natural Sciences, Faculty of Science and Engineering, Macquarie University, Sydney, NSW 2109, Australia*

**Junxian Liu** − *School of Mechanical, Medical and Process Engineering, Queensland University of Technology, Brisbane, Queensland 4001, Australia;* orcid.org/0000-0002-5873-0095

**Yuantong Gu** − *School of Mechanical, Medical and Process Engineering, Queensland University of Technology, Brisbane, Queensland 4001, Australia*

Complete contact information is available at: https://pubs.acs.org/10.1021/jacs.3c11959


### Notes

The authors declare no competing financial interest.

## ACKNOWLEDGMENTS

We would like to appreciate A/Prof. Koushik Venkatesan and Aarti Rajotiya for their support in measuring fluorescence lifetime of samples. We would like to acknowledge Dr. Su Su Thae Hnit for her valuable support in performing the statistical analysis on data. M.T.Y. would like to acknowledge Macquarie University to support this work through Macquarie University Research Fellowship (MQRF). The authors would like to acknowledge the Macquarie University Faculty of Science and Engineering Microscopy Unit for access to its instrumentation and staff. This work was supported by the Australian Research Council (ARC) through the Discovery Projects (DP200102004), and ARC Future Fellowship (FT210100737) to Y.W.

## REFERENCES

(1) Xu, N.; Shi, L.; Pei, X.; Zhang, W.; Chen, J.; Han, Z.; Samorì, P.; Wang, J.; Wang, P.; Shi, Y.; Li, S. Oxidation kinetics and non-Marcusian charge transfer in dimensionally confined semiconductors. *Nat. Commun.* **2023**, *14* (1), 4074.

(2) Favron, A.; Gaufrès, E.; Fossard, F.; Phaneuf-L'Heureux, A.-L.; Tang, N. Y. W.; Lévesque, P. L.; Loiseau, A.; Leonelli, R.; Francoeur,

S.; Martel, R. Photooxidation and quantum confinement effects in exfoliated black phosphorus. *Nat. Mater.* **2015**, *14* (8), 826−832.
(3) Krause, S.; Milić, J. V. Functional dynamics in framework materials. *Commun. Chem.* **2023**, *6* (1), 151.
(4) Homma, K.; Kaneko, S.; Tsukagoshi, K.; Nishino, T. Intermolecular and Electrode-Molecule Bonding in a Single Dimer Junction of Naphthalenethiol as Revealed by Surface-Enhanced Raman Scattering Combined with Transport Measurements. *J. Am. Chem. Soc.* **2023**, *145* (29), 15788−15795.
(5) Zhang, S.; Zheng, H.; Tratnyek, P. G. Advanced redox processes for sustainable water treatment. *Nature Water* **2023**, *1*, 666−681.
(6) Wu, J.; Liu, H.; Chen, W.; Ma, B.; Ju, H. Device integration of electrochemical biosensors. *Nat. Rev. Bioeng.* **2023**, *1* (5), 346−360.
(7) Laing, S.; Jamieson, L. E.; Faulds, K.; Graham, D. Surface-enhanced Raman spectroscopy for in vivo biosensing. *Nat. Rev. Chem* **2017**, *1* (8), 0060.
(8) Boerigter, C.; Aslam, U.; Linic, S. Mechanism of Charge Transfer from Plasmonic Nanostructures to Chemically Attached Materials. *ACS Nano* **2016**, *10* (6), 6108−6115.
(9) Ratchford, D. C. Plasmon-Induced Charge Transfer: Challenges and Outlook. *ACS Nano* **2019**, *13* (12), 13610−13614.
(10) Sarkar, S.; Gupta, V.; Tsuda, T.; Gour, J.; Singh, A.; Aftenieva, O.; Steiner, A. M.; Hoffmann, M.; Kumar, S.; Fery, A.; Joseph, J.; König, T. A. Plasmonic Charge Transfers in Large-Scale Metallic and Colloidal Photonic Crystal Slabs. *Adv. Funct. Mater.* **2021**, *31* (19), 2011099.
(11) Pyo, K.; Matus, M. F.; Hulkko, E.; Myllyperkiö, P.; Malola, S.; Kumpulainen, T.; Häkkinen, H.; Pettersson, M. Atomistic View of the Energy Transfer in a Fluorophore-Functionalized Gold Nanocluster. *J. Am. Chem. Soc.* **2023**, *145* (27), 14697−14704.
(12) Goldmann, C.; Lazzari, R.; Paquez, X.; Boissière, C.; Ribot, F.; Sanchez, C.; Chanéac, C.; Portehault, D. Charge Transfer at Hybrid Interfaces: Plasmonics of Aromatic Thiol-Capped Gold Nanoparticles. *ACS Nano* **2015**, *9* (7), 7572−7582.
(13) Son, J.; Kim, G.-H.; Lee, Y.; Lee, C.; Cha, S.; Nam, J.-M. Toward Quantitative Surface-Enhanced Raman Scattering with Plasmonic Nanoparticles: Multiscale View on Heterogeneities in Particle Morphology, Surface Modification, Interface, and Analytical Protocols. *J. Am. Chem. Soc.* **2022**, *144* (49), 22337−22351.
(14) Tavakkoli Yaraki, M.; Tukova, A.; Wang, Y. Emerging SERS biosensors for the analysis of cells and extracellular vesicles. *Nanoscale* **2022**, *14* (41), 15242−15268.
(15) Nguyen, N. T. T.; Tavakkoli Yaraki, M.; Wang, Y. Enabling spectral barcoding of SERS nanotags using gold nanostars. *Mol. Syst. Des. Eng.* **2023**, *8*, 251−260.
(16) Mantilla, A. B. C.; Wang, C.-F.; Gu, Y.; Schultz, Z. D.; El-Khoury, P. Z. Multipolar Raman Scattering vs Interfacial Nanochemistry: Case of 4-Mercaptopyridine on Gold. *J. Am. Chem. Soc.* **2022**, *144* (45), 20561−20565.
(17) Song, G.; Cong, S.; Zhao, Z. Defect engineering in semiconductor-based SERS. *Chem. Sci.* **2022**, *13* (5), 1210−1224.
(18) Wang, X.; Zhang, E.; Shi, H.; Tao, Y.; Ren, X. Semiconductor-based surface enhanced Raman scattering (SERS): from active materials to performance improvement. *Analyst* **2022**, *147* (7), 1257−1272.
(19) Ding, S.-Y.; You, E.-M.; Tian, Z.-Q.; Moskovits, M. Electromagnetic theories of surface-enhanced Raman spectroscopy. *Chem. Soc. Rev.* **2017**, *46* (13), 4042−4076.
(20) Liang, X.; Liang, B.; Pan, Z.; Lang, X.; Zhang, Y.; Wang, G.; Yin, P.; Guo, L. Tuning plasmonic and chemical enhancement for SERS detection on graphene-based Au hybrids. *Nanoscale* **2015**, *7* (47), 20188−20196.
(21) Liu, B.; Thielert, B.; Reutter, A.; Stosch, R.; Lemmens, P. Quantifying the Contribution of Chemical Enhancement to SERS: A Model Based on the Analysis of Light-Induced Degradation Processes. *J. Phys. Chem. C* **2019**, *123* (31), 19119−19124.
(22) Wen, X.; Yu, P.; Toh, Y.-R.; Lee, Y.-C.; Huang, K.-Y.; Huang, S.; Shrestha, S.; Conibeer, G.; Tang, J. Ultrafast electron transfer in the nanocomposite of the graphene oxide-Au nanocluster with graphene oxide as a donor. *J. Mater. Chem. C* **2014**, *2* (19), 3826−3834.
(23) Deng, H.-H.; Huang, K.-Y.; Zhu, C.-T.; Shen, J.-F.; Zhang, X.-P.; Peng, H.-P.; Xia, X.-H.; Chen, W. Bell-Shaped Electron Transfer Kinetics in Gold Nanoclusters. *J. Phys. Chem. Lett.* **2021**, *12* (2), 876−883.
(24) Huang, K.; Fang, Q.; Sun, W.; He, S.; Yao, Q.; Xie, J.; Chen, W.; Deng, H. Cucurbit[n]uril Supramolecular Assemblies-Regulated Charge Transfer for Luminescence Switching of Gold Nanoclusters. *J. Phys. Chem. Lett.* **2022**, *13* (1), 419−426.
(25) Wang, X.; Liu, G.; Hu, R.; Cao, M.; Yan, S.; Bao, Y.; Ren, B. Chapter 1 - Principles of surface-enhanced Raman spectroscopy. In *Principles and Clinical Diagnostic Applications of Surface-Enhanced Raman Spectroscopy*; Wang, Y., Ed.; Elsevier, 2022, pp 1−32.
(26) Ding, S.-Y.; Yi, J.; Li, J.-F.; Ren, B.; Wu, D.-Y.; Panneerselvam, R.; Tian, Z.-Q. Nanostructure-based plasmon-enhanced Raman spectroscopy for surface analysis of materials. *Nat. Rev. Mater.* **2016**, *1* (6), 16021.
(27) Eremin, Y. A. SCATTERING | Scattering Theory. In *Encyclopedia of Modern Optics*; Guenther, R. D., Ed.; Elsevier: Oxford, 2005, pp 326−330.
(28) Kimling, J.; Maier, M.; Okenve, B.; Kotaidis, V.; Ballot, H.; Plech, A. Turkevich Method for Gold Nanoparticle Synthesis Revisited. *J. Phys. Chem. B* **2006**, *110* (32), 15700−15707.
(29) Haiss, W.; Thanh, N. T. K.; Aveyard, J.; Fernig, D. G. Determination of Size and Concentration of Gold Nanoparticles from UV-Vis Spectra. *Anal. Chem.* **2007**, *79* (11), 4215−4221.
(30) He, Y. Q.; Liu, S. P.; Kong, L.; Liu, Z. F. A study on the sizes and concentrations of gold nanoparticles by spectra of absorption, resonance Rayleigh scattering and resonance non-linear scattering. *Spectrochim. Acta, Part A* **2005**, *61* (13−14), 2861−2866.
(31) Zhou, X.-D.; Li, X.; Shen, A.-G. Chapter 5 - Surface-enhanced Raman scattering nanotags design and synthesis. In *Principles and Clinical Diagnostic Applications of Surface-Enhanced Raman Spectroscopy*; Wang, Y., Ed.; Elsevier, 2022, pp 171−223.
(32) Asadi, M.; Asadi, Z.; Zarei, L.; Sadi, S. B.; Amirghofran, Z. Affinity to bovine serum albumin and anticancer activity of some new water-soluble metal Schiff base complexes. *Spectrochim. Acta, Part A* **2014**, *133*, 697−706.
(33) Samari, F.; Hemmateenejad, B.; Shamsipur, M.; Rashidi, M.; Samouei, H. Affinity of Two Novel Five-Coordinated Anticancer Pt(II) Complexes to Human and Bovine Serum Albumins: A Spectroscopic Approach. *Inorg. Chem.* **2012**, *51* (6), 3454−3464.
(34) Xie, J.; Zheng, Y.; Ying, J. Y. Protein-Directed Synthesis of Highly Fluorescent Gold Nanoclusters. *J. Am. Chem. Soc.* **2009**, *131* (3), 888−889.
(35) Yohannes, G.; Wiedmer, S. K.; Elomaa, M.; Jussila, M.; Aseyev, V.; Riekkola, M.-L. Thermal aggregation of bovine serum albumin studied by asymmetrical flow field-flow fractionation. *Anal. Chim. Acta* **2010**, *675* (2), 191−198.
(36) Tukova, A.; Nie, Y.; Tavakkoli Yaraki, M.; Tran, N. T.; Wang, J.; Rodger, A.; Gu, Y.; Wang, Y. Shape dependent protein-induced stabilization of gold nanoparticles: From a protein corona perspective. *Aggregate* **2023**, *4*, No. e323.
(37) Langer, J.; Jimenez de Aberasturi, D.; Aizpurua, J.; Alvarez-Puebla, R. A.; Auguié, B.; Baumberg, J. J.; Bazan, G. C.; Bell, S. E. J.; Boisen, A.; Brolo, A. G.; Choo, J.; Cialla-May, D.; Deckert, V.; Fabris, L.; Faulds, K.; García de Abajo, F. J.; Goodacre, R.; Graham, D.; Haes, A. J.; Haynes, C. L.; Huck, C.; Itoh, T.; Käll, M.; Kneipp, J.; Kotov, N. A.; Kuang, H.; Le Ru, E. C.; Lee, H. K.; Li, J.-F.; Ling, X. Y.; Maier, S. A.; Mayerhöfer, T.; Moskovits, M.; Murakoshi, K.; Nam, J.-M.; Nie, S.; Ozaki, Y.; Pastoriza-Santos, I.; Perez-Juste, J.; Popp, J.; Pucci, A.; Reich, S.; Ren, B.; Schatz, G. C.; Shegai, T.; Schlücker, S.; Tay, L.-L.; Thomas, K. G.; Tian, Z.-Q.; Van Duyne, R. P.; Vo-Dinh, T.; Wang, Y.; Willets, K. A.; Xu, C.; Xu, H.; Xu, Y.; Yamamoto, Y. S.; Zhao, B.; Liz-Marzán, L. M. Present and Future of Surface-Enhanced Raman Scattering. *ACS Nano* **2020**, *14* (1), 28−117.
(38) Pienpinijtham, P.; Kitahama, Y.; Ozaki, Y. Electric field analysis, polarization, excitation wavelength dependence, and novel applica-


https://doi.org/10.1021/jacs.3c11959
J. Am. Chem. Soc. 2024, 146, 5916−5926

tions of tip-enhanced Raman scattering. *J. Raman Spectrosc.* **2021**, *52* (12), 1997−2017.
(39) Andrews, D. L.; Blake, N. P. Electric-field-induced Raman spectroscopy. *J. Chem. Phys.* **1988**, *88* (10), 6039−6048.
(40) van der Vaart, A.; Merz, K. M. The Role of Polarization and Charge Transfer in the Solvation of Biomolecules. *J. Am. Chem. Soc.* **1999**, *121* (39), 9182−9190.
(41) Bartashevich, E. V.; Tsirelson, V. G. Atomic dipole polarization in charge-transfer complexes with halogen bonding. *Phys. Chem. Chem. Phys.* **2013**, *15* (7), 2530−2538.
(42) Ye, J.; Hutchison, J. A.; Uji-i, H.; Hofkens, J.; Lagae, L.; Maes, G.; Borghs, G.; Van Dorpe, P. Excitation wavelength dependent surface enhanced Raman scattering of 4-aminothiophenol on gold nanorings. *Nanoscale* **2012**, *4* (5), 1606−1611.
(43) Shan, Y.; Zheng, Z.; Liu, J.; Yang, Y.; Li, Z.; Huang, Z.; Jiang, D. Niobium pentoxide: a promising surface-enhanced Raman scattering active semiconductor substrate. *npj Comput. Mater.* **2017**, *3* (1), 11.
(44) Cui, L.; Wu, D.-Y.; Wang, A.; Ren, B.; Tian, Z.-Q. Charge-Transfer Enhancement Involved in the SERS of Adenine on Rh and Pd Demonstrated by Ultraviolet to Visible Laser Excitation. *J. Phys. Chem. C* **2010**, *114* (39), 16588−16595.
(45) Richter, A. P.; Lombardi, J. R.; Zhao, B. Size and Wavelength Dependence of the Charge-Transfer Contributions to Surface-Enhanced Raman Spectroscopy in Ag/PATP/ZnO Junctions. *J. Phys. Chem. C* **2010**, *114* (3), 1610−1614.
(46) Ji, W.; Li, L.; Song, W.; Wang, X.; Zhao, B.; Ozaki, Y. Enhanced Raman Scattering by ZnO Superstructures: Synergistic Effect of Charge Transfer and Mie Resonances. *Angew. Chem., Int. Ed.* **2019**, *58* (41), 14452−14456.
(47) Zhu, W.; Hutchison, J. A.; Dong, M.; Li, M. Frequency Shift Surface-Enhanced Raman Spectroscopy Sensing: An Ultrasensitive Multiplex Assay for Biomarkers in Human Health. *ACS Sens.* **2021**, *6* (5), 1704−1716.
(48) Ma, H.; Liu, S.; Zheng, N.; Liu, Y.; Han, X. X.; He, C.; Lu, H.; Zhao, B. Frequency Shifts in Surface-Enhanced Raman Spectroscopy-Based Immunoassays: Mechanistic Insights and Application in Protein Carbonylation Detection. *Anal. Chem.* **2019**, *91* (15), 9376−9381.
(49) Wang, Y.; Ji, W.; Sui, H.; Kitahama, Y.; Ruan, W.; Ozaki, Y.; Zhao, B. Exploring the Effect of Intermolecular H-Bonding: A Study on Charge-Transfer Contribution to Surface-Enhanced Raman Scattering of p-Mercaptobenzoic Acid. *J. Phys. Chem. C* **2014**, *118* (19), 10191−10197.
(50) Wang, Y.; Liu, J.; Ozaki, Y.; Xu, Z.; Zhao, B. Effect of TiO2 on Altering Direction of Interfacial Charge Transfer in a TiO2-Ag-MPY-FePc System by SERS. *Angew. Chem., Int. Ed.* **2019**, *58* (24), 8172−8176.
(51) Zhang, X.; Sui, H.; Wang, X.; Su, H.; Cheng, W.; Wang, X.; Zhao, B. Charge transfer process at the Ag/MPH/TiO2 interface by SERS: alignment of the Fermi level. *Phys. Chem. Chem. Phys.* **2016**, *18* (43), 30053−30060.
(52) Park, W.-H.; Kim, Z. H. Charge Transfer Enhancement in the SERS of a Single Molecule. *Nano Lett.* **2010**, *10* (10), 4040−4048.
(53) Yun, C. S.; Javier, A.; Jennings, T.; Fisher, M.; Hira, S.; Peterson, S.; Hopkins, B.; Reich, N. O.; Strouse, G. F. Nanometal Surface Energy Transfer in Optical Rulers, Breaking the FRET Barrier. *J. Am. Chem. Soc.* **2005**, *127* (9), 3115−3119.
(54) Tavakkoli Yaraki, M.; Pan, Y.; Hu, F.; Yu, Y.; Liu, B.; Tan, Y. N. Nanosilver-enhanced AIE photosensitizer for simultaneous bioimaging and photodynamic therapy. *Mater. Chem. Front.* **2020**, *4* (10), 3074−3085.
(55) Tavakkoli Yaraki, M.; Wu, M.; Middha, E.; Wu, W.; Daqiqeh Rezaei, S.; Liu, B.; Tan, Y. N. Gold Nanostars-AIE Theranostic Nanodots with Enhanced Fluorescence and Photosensitization Towards Effective Image-Guided Photodynamic Therapy. *Nano-Micro Lett.* **2021**, *13* (1), 58.
(56) Li, J.-F.; Li, C.-Y.; Aroca, R. F. Plasmon-enhanced fluorescence spectroscopy. *Chem. Soc. Rev.* **2017**, *46* (13), 3962−3979.
(57) Wilbraham, L.; Smajli, D.; Heath-Apostolopoulos, I.; Zwijnenburg, M. A. Mapping the optoelectronic property space of small aromatic molecules. *Commun. Chem.* **2020**, *3* (1), 14.
(58) Cao, J.; Zhang, H.; Pi, X.; Li, D.; Yang, D. Enhanced photoluminescence of silicon quantum dots in the presence of both energy transfer enhancement and emission enhancement mechanisms assisted by the double plasmon modes of gold nanorods. *Nanoscale Adv.* **2021**, *3* (16), 4810−4815.
(59) Poirier-Richard, H. P.; Couture, M.; Brule, T.; Masson, J. F. Metal-enhanced fluorescence and FRET on nanohole arrays excited at angled incidence. *Analyst* **2015**, *140* (14), 4792−4798.
(60) Wang, Y.; Zou, X.; Ren, W.; Wang, W.; Wang, E. Effect of Silver Nanoplates on Raman Spectra of p-Aminothiophenol Assembled on Smooth Macroscopic Gold and Silver Surface. *J. Phys. Chem. C* **2007**, *111* (8), 3259−3265.
(61) Wang, Y.; Chen, H.; Dong, S.; Wang, E. Surface enhanced Raman scattering of p-aminothiophenol self-assembled monolayers in sandwich structure fabricated on glass. *J. Chem. Phys.* **2006**, *124*(7)..
(62) Osawa, M.; Matsuda, N.; Yoshii, K.; Uchida, I. Charge transfer resonance Raman process in surface-enhanced Raman scattering from p-aminothiophenol adsorbed on silver: Herzberg-Teller contribution. *J. Phys. Chem.* **1994**, *98* (48), 12702−12707.
(63) Zhou, Q.; Li, X.; Fan, Q.; Zhang, X.; Zheng, J. Charge Transfer between Metal Nanoparticles Interconnected with a Functionalized Molecule Probed by Surface-Enhanced Raman Spectroscopy. *Angew. Chem., Int. Ed.* **2006**, *45* (24), 3970−3973.
(64) Clark, R. J. H.; Dines, T. J. Resonance Raman Spectroscopy, and Its Application to Inorganic Chemistry. New Analytical Methods (27). *Angew Chem. Int. Ed. Engl.* **1986**, *25* (2), 131−158.
(65) Cong, S.; Liu, X.; Jiang, Y.; Zhang, W.; Zhao, Z. Surface Enhanced Raman Scattering Revealed by Interfacial Charge-Transfer Transitions. *Innovation* **2020**, *1* (3), 100051.


https://doi.org/10.1021/jacs.3c11959
J. Am. Chem. Soc. 2024, 146, 5916−5926